

Tuning the magnetic state in a phase-separated magnetic oxide thin film by means of electric field and temperature

O. G. Udalov^{1,2,3} and I. S. Beloborodov¹

¹*Department of Physics and Astronomy, California State University Northridge, Northridge, California 91330, USA*

²*Institute for Physics of Microstructures RAS, 603950 Nizhny Novgorod, Russia*

³*Lobachevsky State University of Nizhny Novgorod, 603950 Nizhny Novgorod, Russia*



(Received 16 March 2020; accepted 6 May 2020; published 21 May 2020)

We study a hybrid system of a magnetic oxide thin film on a ferroelectric substrate. We show that magnetic and transport properties of the magnetic oxide film strongly depend on the dielectric constant and polarization of the ferroelectric substrate. Tuning these parameters one can induce the metal-insulator transition in the magnetic oxide film accompanied by the ferromagnetic to superparamagnetic transition. Ferroelectric properties can be tuned by varying temperature or applying an electric field.

DOI: [10.1103/PhysRevB.101.174433](https://doi.org/10.1103/PhysRevB.101.174433)

I. INTRODUCTION

Hybrid ferroelectric (FE)/ferromagnetic (FM) systems attract a lot of attention nowadays [1–7]. They demonstrate a magnetoelectric (ME) effect promising numerous novel microelectronic, micromechanical, and biomedical applications [2,8–11]. FE materials are sensitive to an electric field and can affect the FM layer either through the strain (magnetoelastic effect) [5–7,12–14] or charge accumulation in the FM layer [13,15–17]. Recently another mechanism of the ME effect was proposed related to dielectric properties of FEs [18–20]. In particular, the FE can screen the Coulomb interaction in a granular magnetic film leading to renormalization of the intergrain exchange interaction. Changing the FE dielectric constant using an electric field or temperature one can switch the magnetic film state from the FM one to the superparamagnetic (SPM) one.

In a granular magnet, metallic FM nanograins are dispersed in an insulating nonmagnetic matrix. Interestingly, that similar situation may appear in magnetic oxides (MOs). The physics of these materials is quite complicated and intriguing with many competing phenomena [21–26]. One of the most striking features of MOs is the appearance of the so-called phase-separated (PS) state [27–31]. In this state the material is split into FM conductive clusters and antiferromagnetic (AFM) insulating regions. The size and the distance between the FM clusters are defined by the system internal parameters, in contrast to the case of granular magnets where the grain size and the intergrain distance are defined during the fabrication process. What is important is that the PS state shows a charge separation as well. The FM clusters are negatively charged while the AFM regions are positively charged. Due to the charge separation phenomena the Coulomb interaction essentially affects the system state. This opens the way to manipulate the system state through the controllable screening of the Coulomb interaction in the same manner as was proposed for granular magnets and diluted magnetic ferroelectrics [18–20,32].

In MO/FE systems the Coulomb-based ME effect is expected to work as follows. In the PS state the MO film has conductive and insulating regions. Depending on the volume ratio of these phases the whole system can be either conductive FM or insulating SPM. The Coulomb interaction favors the uniform distribution of charges and therefore it favors the non-PS uniform conductive state. In the case of strong Coulomb interaction the system should be in a uniform state, while in the case of weak Coulomb interaction the system tends to form the PS insulating state. The strength of the Coulomb interaction can be tuned via screening. The electric field produced by the PS MO film is screened by the FE substrate. If the screening is strong enough (meaning that the dielectric constant ϵ is high), the Coulomb interaction is weak and we get the insulating PS MO film. If the screening is weak (meaning that the dielectric constant ϵ is low) we have the conducting FM MO film. In FEs the dielectric constant can be tuned with voltage or temperature. FEs have a strong peak of the dielectric constant close to the Curie temperature. One can expect that in this region there is a metal-to-insulator (MIT) transition in MO/FE systems. This transition is accompanied by the FM-to-SPM transition. Far from the Curie point the dielectric constant ϵ is low leading to the uniform FM conductive state. At the Curie point ϵ is high and the insulating PS SPM state can appear. Similarly, the FE dielectric constant depends on the applied voltage. This case is shown in Fig. 1. When a large voltage is applied across the FE substrate the dielectric constant is low and the state with large overlap of FM clusters is formed leading to the conductive FM state (see the upper panel). For zero applied voltage the dielectric constant is large and the separated clusters appear forming the insulating PS state. The transition between these two states is of percolation type.

Besides the ME effect mediated by the FE dielectric constant, the charge accumulation based ME coupling can occur in the MO/FE system. The charge accumulation in a MO film may appear at finite voltage applied to the FE. The voltage

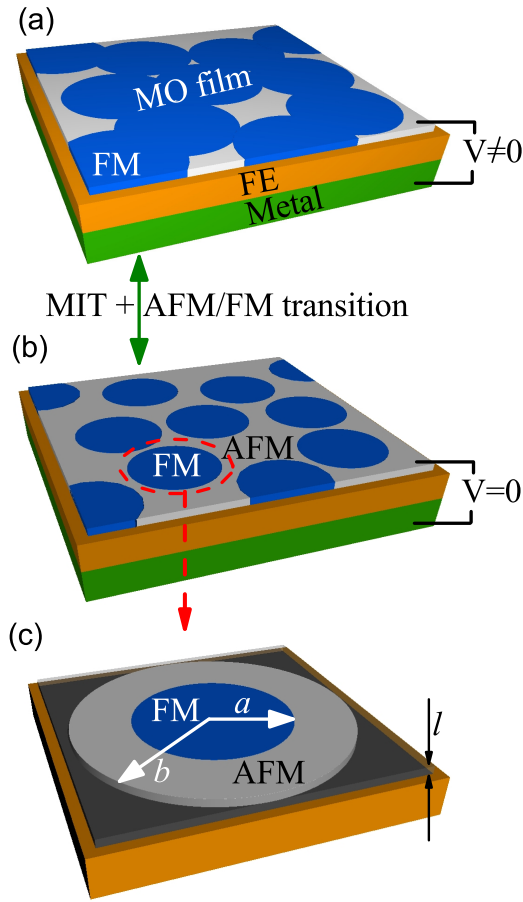


FIG. 1. FE substrate (orange) sandwiched between metal electrode and the PS MO film with FM conducting clusters and AFM insulating regions. (a) Nonzero voltage is applied to the FE. The FM clusters are big enough. They overlap forming an infinite conductive FM network. (b) Zero-voltage limit. The FM clusters are small and separated by the insulating AFM regions. The whole film is an insulator and a SPM. (c) A single FM cluster surrounded by the AFM ring. a is the average FM cluster radius, $2b$ is the average distance between the FM clusters, and l is the MO film thickness.

induces a variation of the electron density in the MO film changing in its turn the system magnetic state. Moreover, the FE has an electric polarization which can be switched by an electric field pulse. Switching the polarization should also change the electron density in the MO film and eventually change its magnetic state. This opens an additional way to control the MO film. In this work we consider both effects: (i) the effect of polarization and (ii) the effect of dielectric constant on the MO film behavior.

The paper is organized as follows. Sec. II discusses the model of the hybrid MO/FE system. In Sec. III we consider a simplified model and study it analytically. In the next section we use numerical simulations to investigate the Hamiltonian and discuss the MO film behavior depending on the dielectric constant and polarization of the FE substrate. In the discussion section, Sec. V, we address the relevant materials and model limitations.

II. THE MODEL

We consider a thin MO film with the thickness of l measured in the numbers of atomic planes. The interatomic distance is denoted Δ . The film is a perfect crystal placed on top of a FE substrate (see Fig. 1). The substrate has a dielectric constant ϵ and polarization P depending on temperature T and external electric field E .

We use the double exchange model with a single orbital per site, “classic” magnetic moments, and a cubic lattice to describe magnetic and electronic properties of the MO layer [28,31]. The Hamiltonian of the system has the form

$$\hat{H} = - \sum_{(i,j)} t_{ij} \hat{a}_i^\dagger \hat{a}_j + \text{c.c.} - J \sum_{(i,j)} \mathbf{S}_i \mathbf{S}_j + \hat{H}_C, \quad (1)$$

where the first two terms are the electron kinetic energy with \hat{a}_i and \hat{a}_i^\dagger being the creation and annihilation operators for an electron at the site i . The transfer matrix element t_{ij} depends on the mutual orientation of magnetic moments of sites i and j , $t_{ij} = t \cos(\theta_{ij}/2)$, where $\theta_{ij} = \hat{\mathbf{S}}_i \hat{\mathbf{S}}_j$. The third term in Eq. (1) describes the exchange interaction of magnetic ions. The classical vector \mathbf{S}_i is the magnetic moment (normalized) of the i site; $J < 0$ is the (AFM) intersite exchange coupling. The summation in all three of these terms is performed over the nearest neighbors.

The last term in Eq. (1) is the Coulomb interaction including electron-electron, electron-ion, ion-ion, electron-FE, and ion-FE contributions. The FE substrate is considered as a uniform media with a given dielectric constant ϵ . It screens the electric field produced by electrons and ions. The charge inhomogeneity appears in a phase-separated MO film. It creates a stray electric field penetrating to and interacting with the FE substrate. The Coulomb interaction can be written as

$$\hat{H}_C = \frac{1}{2} \iint d^3 r_1 d^3 r_2 \rho^{\text{tot}}(\mathbf{r}_1) \rho^{\text{tot}}(\mathbf{r}_2) / (|\mathbf{r}_1 - \mathbf{r}_2|), \quad (2)$$

where ρ^{tot} is the total charge density defined in the MO film as well as in the FE substrate. Inside the MO, the inhomogeneous distribution of electrons and ions contributes to ρ^{tot} . In the FE substrate, the interfacial bound charges induced by the stray field will define the charge density, ρ^{tot} .

III. SIMPLIFIED ANALYTICAL CONSIDERATION

Consider a system with average electron density n_0 electrons per one site. Assume that electrons gather together in disks (we will call them FM regions or clusters) of radius a [see Fig. 1(c)]. The number of the clusters in the film is N_{cl} and the total film area is S . These disks in total fill a part of the film $\xi = N_{\text{cl}} \pi a^2 / S < 1$ (compression ratio). On average the cluster with the radius a is surrounded by the AFM region with the radius $b = a / \sqrt{\xi}$ [see Fig. 1(c)]. Here we consider such a single cluster neglecting other FM regions. We call the FM cluster with the surrounding AFM ring the PS region. The applicability of this assumption is discussed below. The number of electrons in the PS region is N and the electron density is $n = n_0 / \xi$. There cannot be more than 1 electron per site, $n \leq 1$. Therefore, there is a bottom boundary for

the compression ratio $\xi > n_0$. Outside the disks there are no electrons and the state is AFM ($\theta_{ij} = \pi$). Inside the disks there is a canted FM or pure FM state with the angle $\theta_{ij} = \theta < \pi$. The angle is the same for all neighbors.

The single electron spectrum in the disk is given by

$$\epsilon(\mathbf{k}) = -2t \cos(\theta/2) [\cos(k_x \Delta) + \cos(k_y \Delta) + \cos(k_z \Delta)], \quad (3)$$

where $k_{x,y,z}$ are the electron quasimomentums. The total kinetic energy of electrons is calculated as

$$E_k^{\text{tot}} = \frac{\Delta^3}{8\pi^3} \int_{E < E_F} \epsilon(\mathbf{k}) d^3k, \quad (4)$$

where $E_F(n)$ is the Fermi energy defined by the electron density in the cluster growing with reducing of ξ . When n reaches 1 ($\xi = 1/n_0$) all energy levels are occupied and the total kinetic electron energy becomes $E_k^{\text{tot}} = 0$. When the electron concentration is low in the FM droplet ($n \ll 1$, $\xi \gg n_0$) each electron has a kinetic energy on the order of $-6t \cos(\theta/2)$. The total kinetic energy per one site in this case is $-6tn \cos(\theta/2) a^2/b^2 = -6tn_0 \cos(\theta/2)$.

The magnetic energy of the system can be estimated in the following way. Each site in the system has 6 neighbors (we neglect the fact that the number of neighbors for interfacial sites is lower for now). Let us choose the AFM state as the state with a zero energy. Therefore, in the AFM region all sites have zero energy. In the cluster each site has the energy $12|J| \cos(\theta)/2 = 6|J|$ (1/2 is to avoid a double counting). The total magnetic energy is given by $E_m^{\text{tot}} = 6|J| \cos(\theta) a^2/b^2 N = 6|J| \xi \cos(\theta) N$.

The Coulomb energy is estimated as follows. We assume that the charged disk can be considered as an infinitely thin one with the surface charge density

$$\sigma_d(\mathbf{r}_\perp) = \begin{cases} \sigma_1 + \sigma_2, & |\mathbf{r}_\perp| < a, \\ \sigma_2, & a < |\mathbf{r}_\perp| < b, \end{cases} \quad (5)$$

where $\sigma_2 = |e|n_0 l/\Delta^2$ (ion charge density) and $\sigma_1 = -\sigma_2/\xi$ (electron charge density), \mathbf{r}_\perp is the radius vector in the (x, y) plane (the plane of the MO film), and z is the coordinate perpendicular to the film plane. We assume that the considered PS region (including both the FM cluster and AFM ring) does not interact with outer area. The PS region itself is neutral and does not have a dipole moment. It has a quadrupole moment only. Therefore, the interaction between different PS regions decays with distance as $1/r^5$ (r is the distance between the two different FM clusters). In a two-dimensional system we can consider this interaction as a short range. So, we can treat a single PS region neglecting the other ones.

The next assumption is that the disk is thin and is exactly at the interface between the FE (with the dielectric constant ϵ) and surrounding medium (with the dielectric constant equal to 1). In this case, the Coulomb energy of the system is given by

$$E_C = \frac{1}{(1 + \epsilon)} [U_d(a, a, \sigma_1, \sigma_1) + U_d(b, b, \sigma_2, \sigma_2) - 2U_d(a, b, \sigma_1, \sigma_2)], \quad (6)$$

where

$$U_d(r_1, r_2, s_1, s_2) = 2\pi s_1 s_2 \int_0^{r_1} \int_0^{r_2} \int_0^{2\pi} d\chi_1 d\chi_2 d\theta \times \frac{\chi_1 \chi_2}{\sqrt{\chi_1^2 + \chi_2^2 - 2\chi_1 \chi_2 \cos(\theta)}}. \quad (7)$$

Here U_d is the Coulomb interaction of two infinitely thin disks with radii $r_{1,2}$, the surface charge densities $s_{1,2}$, and the same center. We introduce the characteristic Coulomb energy scale $U_0 = |e|^2/\Delta$.

The total energy of the system is the sum of the three contributions described above:

$$E^{\text{tot}} = E_k^{\text{tot}} + E_m^{\text{tot}} + E_C. \quad (8)$$

The dependence of these energies on the size of the FM cluster is shown in Fig. 2. The upper panel shows the behavior of each energy separately. The curves are plotted for the following parameters: $n_0 = 0.05$, $J = 0.015t$, $U_0 = t$, $\epsilon = 1000$, $b = 100\Delta$, and $l = 10$. The energies are shown after the minimization over the angle θ .

In the case of the uniform state ($\xi = 1$), there is a canted FM state in the whole system. The angle θ decreases [$\cos(\theta)$ increases] with decreasing of the compression ratio ξ (see green dash-dotted line). The canted FM state remains in the FM cluster until the compression ratio reaches the critical value $\xi = \xi_{\text{FM}}$. For $\xi < \xi_{\text{FM}}$ no canting remains and the pure FM state occurs in the cluster. The approximate area of the FM region (blue circle) and the surrounding AFM area (gray shell) is shown in the figure.

Energies are plotted in the range between $\xi = 1$ (uniform state, no compression) and $\xi = \xi_{\text{min}} = n_0$ (maximum compression, $n = 1$ in the FM region). The red line represents the kinetic energy. In the canted state ($\xi > \xi_{\text{FM}} \approx 0.6$) the kinetic energy decreases with ξ because the conduction band becomes wider leading to a reducing of the kinetic energy. Namely, the reduction of the electron kinetic energy is responsible for the formation of the PS state. For $\xi < \xi_{\text{FM}}$ the kinetic energy increases since the bandwidth reaches its maximum and further cluster size reduction just increases the electron concentration pushing the electrons to higher and higher energy levels. Finally, when the compression ratio reaches the maximum, $\xi = \xi_{\text{min}}$, the whole band is occupied. The band is symmetric with respect to zero energy. Therefore, the kinetic energy of electrons becomes zero.

We note that for n large enough, $n \approx 0.5$, the single-particle picture does not work well since the correlation effects become important. Therefore, we cannot consider the case with large compression.

The magnetic energy (blue line) behaves in the opposite way: It grows with the reduction of ξ for $\xi > \xi_{\text{FM}}$ and decays for $\xi < \xi_{\text{FM}}$. Since the magnetic energy favors the AFM state it grows with decreasing angle θ ($\xi > \xi_{\text{FM}}$). For $\xi < \xi_{\text{FM}}$ the magnetic energy decays since the area of the FM region decreases linearly with ξ .

The Coulomb energy [black line in the panel (a)] monotonically increases with decreasing ξ , since the charge separation grows and the electric field induced by the charges grows too.

Competition between these three energies leads to the dependence of the system state on the compression ratio

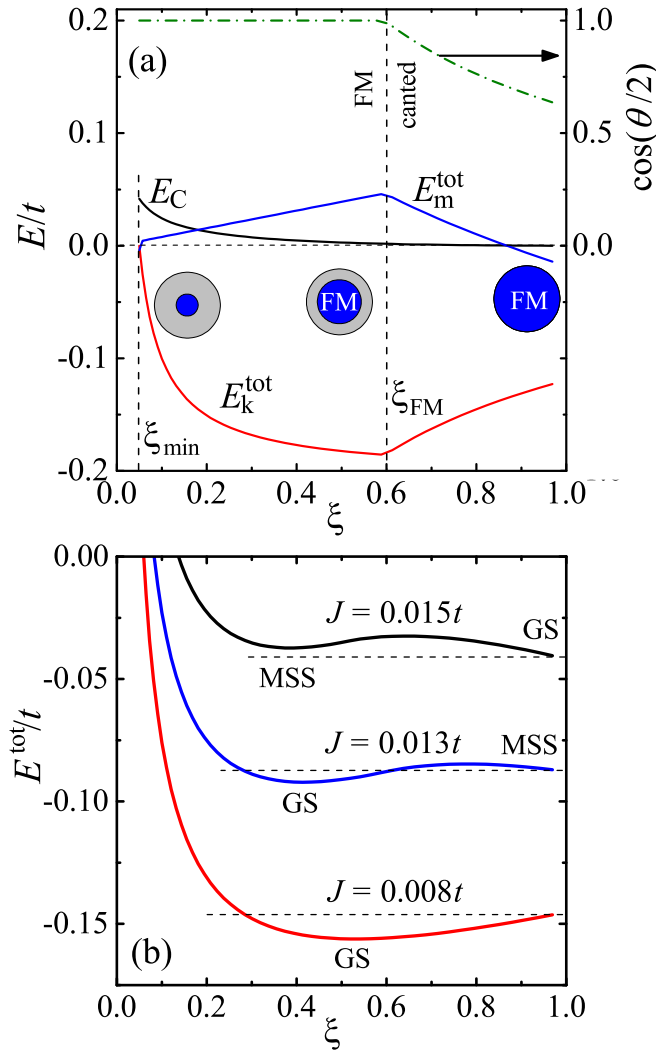


FIG. 2. (a) Electron kinetic energy (E_k^{tot}), magnetic energy (E_m^{tot}), and the Coulomb interaction energy (E_C) as functions of compression ratio ξ . The curves are plotted for the following parameters: $n_0 = 0.05$, $J = 0.015t$, $U_0 = t$, $\varepsilon = 1000$, $b = 100\Delta$, and $l = 10$. Green dash-dotted line shows the dependence of the $\cos(\theta/2)$ on ξ . At $\xi = \xi_{\text{min}} \approx 0.05$ the electron density in the FM cluster reaches 1. Therefore, below this point there is no data for the energies. Circles show a variation of the FM cluster size (gray rings, AFM region; blue circle, FM cluster). (b) Total system energy E^{tot} as a function of compression ratio ξ for different system parameters. All parameters are the same as for panel (a) except J varying from $0.008t$ to $0.015t$. The notation GS is used for the ground state; MSS stands for the metastable state.

and other system parameters. Increasing the film thickness l enhances the Coulomb contribution since $E_C \sim l^2$. At that, E_k^{tot} and E_m^{tot} grow linearly $\sim l^1$. Increasing n_0 also enhances the Coulomb energy since $E_C \sim n_0^2$, while $E_k^{\text{tot}} \sim n_0^1$ and E_m^{tot} is independent of n_0 .

Figure 2(b) shows the total system energy vs ξ . Three different scenarios are shown. The parameters are the same as in Fig. 2(a) except that the exchange constant J varies from $0.008t$ to $0.015t$. At small J there is only one minimum corresponding to the ground state. This minimum occurs at $\xi < 1$, meaning that the PS state is the ground state (GS)

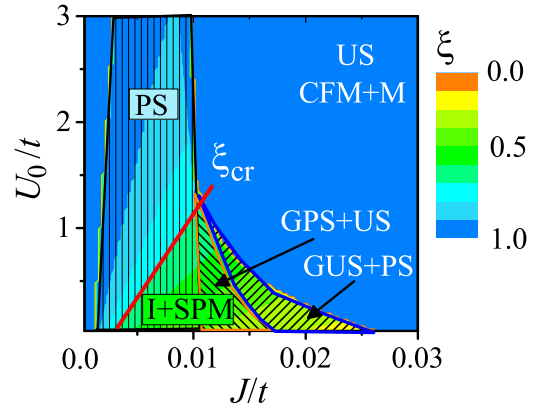


FIG. 3. Dependence of the equilibrium compression ratio ξ on the normalized J and U_0 for given $n_0 = 0.05$, $l = 6$, $b = 50\Delta$, $\varepsilon = 50$. Notation US stands for the uniform state ($\xi = 1$). The letter G in front of any contraction means that the corresponding state is the ground one. The area shaded with vertical lines shows the parameters for which the only equilibrium system state is the PS one. The region shaded with left-leaning lines shows the case when both the PS and US are equilibrium states, but the PS one has the lowest energy. The region GUS + PS indicates the opposite situation. The unshaded blue area is for the case when US is the only equilibrium state in the system. The red line shows the critical density of clusters corresponding to the percolation in a 2D system with a random cluster arrangement. Notation I + SPM stands for the insulating superparamagnetic state; CFM + M is for the canted ferromagnetic metallic state.

of the system. At larger J , two stable states may appear. The first one is the PS state ($\xi < 1$) and the second one is the uniform state (US; $\xi = 1$). Depending on J either of these states could be the ground one. At intermediate J the PS state is the ground one (blue line). For higher J the US becomes the state with the lowest energy (black line). For even larger J , the PS metastable state disappears and only the US exists. Thus, for large J the PS state cannot be realized. This happens because for large J the growth of the magnetic energy due to phase separation cannot be compensated by the decrease of the electron kinetic energy.

Figure 3 shows the typical phase diagram (PD) of the system. It shows the dependence of the equilibrium compression ratio ξ on J/t and U_0/t for a given $n_0 = 0.05$, $l = 6$, $b = 50\Delta$, $\varepsilon = 50$. Several regions are visible on this phase diagram. The unshaded blue region corresponds to the situation when only the US ($\xi = 1$) is realized in the system. The shaded area marked as GUS + PS corresponds the system with ground US and metastable PS state [the black line in Fig. 2(b)]. The shaded area bordered with the orange line (GPS + US) shows the opposite case when the PS state is the ground one [the blue line in Fig. 2(b)]. The region with vertical lines (PS) corresponds to the case when only the PS state is realized in the MO film [the red line in Fig. 2(b)].

In general the compression ratio ξ grows with increasing the Coulomb energy U_0 . The larger the Coulomb interaction the more difficult it is to separate charges. A strong exchange coupling J also favors the uniform canted ferromagnetic metallic (CFM + M) state. The ground state in the GUS + PS parameter region also corresponds to the conductive FM state.

The PS state can be considered as an insulating and SPM state (I + SPM). However, for large enough compression ratio the FM clusters can overlap and form an infinite conductive FM network. For random distribution of FM regions the percolation appears at the critical compression ratio, $\xi_{cr} = 0.65$ (see discussion of the percolation problem in Sec. VB). This critical value is shown in Fig. 3 with the red line. Below this line an insulating state exists while above this line the conductive state is more probable.

A transition between conductive FM and insulating SPM states may occur by tuning parameters of the FE substrate. For example, varying temperature one can tune the dielectric constant of the FE material. In the vicinity of the FE phase transition the dielectric constant increases sharply and can grow by an order of magnitude (see Sec. VA for discussions). Such a growth reduces the Coulomb interaction and can be considered as moving down along the phase diagram toward smaller U_0 .

Another way to control the system is to apply an electric field switching the FE polarization, \mathbf{P} (see Fig. 1). If the polarization direction is perpendicular to the MO film surface, the switching will modify the electron concentration in the MO layer. The FE polarization will create an internal electric field inside the FE layer. Depending on the polarization direction the field may have an opposite sign. For zero voltage across the FE, the internal electric field is screened by charges in the MO film (and bottom electrode). Therefore, depending on the polarization direction one can have electron accumulation or depletion in the MO layer. Polarization switching can be realized by the field pulse of certain polarity. After the switching, the voltage is zero and there is no electric field in the FE. The polarization changes by $2P_0$, where P_0 is the remnant polarization of the FE. The electron density per site varies by $2P_0\Delta^2/l$. For film with thickness of 6 monolayers, the charge density variation per one site can be from $\Delta n_0 = 0.025$ to $\Delta n_0 = 0.05$ for typical FEs (see Sec. VA for a discussion of materials).

One more way to change the parameters of the FE substrate is to apply a constant electric field modifying both the electric polarization and the dielectric constant. For high enough applied field the polarization is saturated. Since the FE has a nonlinear relation between a polarization and an electric field, the dielectric constant is a function of applied voltage. The dielectric constant usually decreases with the electric field and may fall down several times (see Sec. VA).

Figure 4 shows the phase diagram of MO/FE system vs FE parameters. All the PDs are plotted for $l = 6$ and $b = 50\Delta$. The upper row in Fig. 4 shows what happens if the dielectric constant varies from 50 to 500 (real numbers for TTF-CA FE near the Curie point). The gray color shows the region where the PS state appears. The red line borders the region where the FM cluster total area is below the percolation threshold for 2D systems ($\xi < 0.65$). In this region an I + SPM state exists. In the rest of the gray area the percolation leads to the appearance of the infinite cluster network. Therefore, this region corresponds to the FM conductive state. Increasing of the dielectric constant enlarges the region where the I + SPM state exists. Thus, tuning the temperature one can transform the system from the metallic (FM) to insulating (SPM) phase.

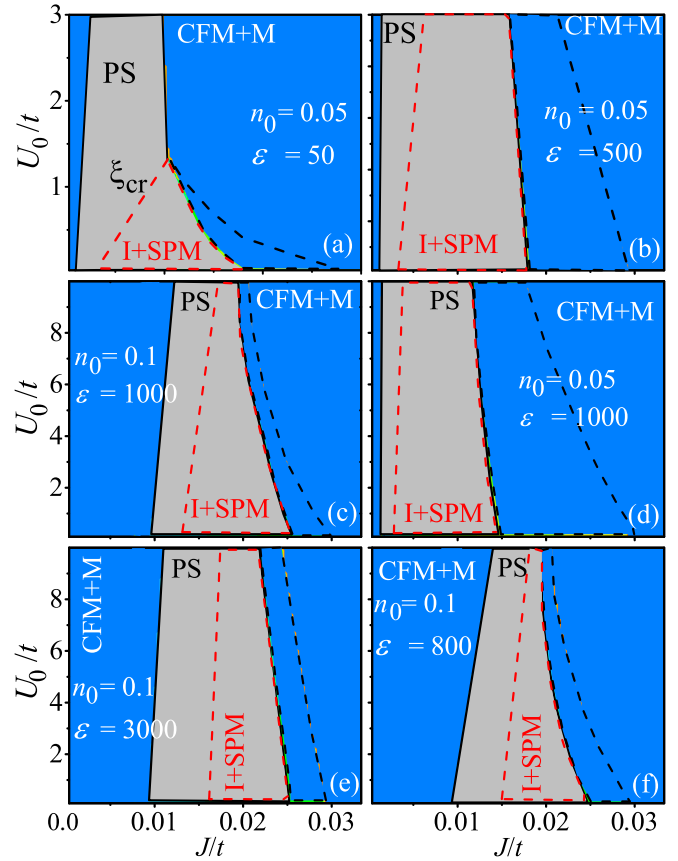


FIG. 4. Phase diagram of MO/FE system in coordinates J/t and U_0/t for given $l = 6$, $b = 50\Delta$. Gray area shows the PS state ($\xi < 1$). Blue area is the region where the US is the ground state ($\xi = 1$). In this region the canted FM metallic state (CFM + M) is realized. The black dashed line shows the region where the ground state is a uniform state but the PS state is metastable. The red dashed line borders the region in which the total area of the FM clusters is below the 2D percolation threshold. Inside the red border the insulating superparamagnetic state (I + SPM) is realized. In the rest of the gray area FM clusters form an infinite FM cluster covering the whole system and making the MO film conductive. Different panels correspond to different system parameters.

The next row shows what happens when polarization of the FE switches. Two panels correspond to two different electron densities $n_0 = 0.5$ and $n_0 = 0.1$. The electron density variation corresponds to the switching of a FE with the remnant polarization of $10 \mu\text{C}/\text{cm}^2$. Polarization switching can substantially modify the phase diagram leading to the MIT transition.

The last row shows the case when a constant electric field is applied and the dielectric constant of the FE changes from 3000 to 800. This change is typical for KTiO_3 . In this case the MIT transition can be achieved as well.

Limitations of analytical model

The main limitation of the analytical model is that it does not allow us to optimize parameter b which is the average distance between the FM clusters. In our model the kinetic and magnetic energies depend on the parameter $\xi = a^2/b^2$

only. So, for fixed ξ one can change b in any way and this would not influence the magnetic and kinetic energies. The Coulomb interaction scales with ξ and b as $U_C \sim \tilde{U}(\xi)b^2$. Fixing parameter ξ one can reduce b and therefore reduce the total energy of the system. Thus, the parameter b should go to zero in the analytical model which is nonphysical. The reason for such a behavior is that the model does not take into account the surface effects at the boundary between AFM and FM regions and at the film surface. These effects linearly depend on the parameter b . Thus, the smaller the FM cluster size the more pronounced the influence of the surface effects. Eventually, the energy contribution due to the surface effects should overcome the volume contribution. This will limit the reduction of the parameter b . Below we take the surface effects into account in our numerical simulations. In particular, we treat the magnetic energy correctly by considering a domain wall between AFM and FM regions, and by treating film surfaces in a correct way. This increases the energy of the FM cluster. The second effect in our numerical simulations is the influence of the cluster boundaries on the electron spectrum (spectrum modification and energy quantization). Also we consider the influence of the Coulomb interaction on the electron behavior in the FM cluster by taking into account the fact that the wave function changes under the influence of the Coulomb interaction.

IV. NUMERICAL MODELING

A. Modeling procedure

We treat the Hamiltonian in Eq. (1) using numerical simulations. In particular, we consider a finite rectangular PS area in a MO thin film. Inside the area there are two regions: (1) the AFM one without carriers and (2) the FM one containing all electrons; see Fig. 5. Outside the rectangular area the state of the MO film is the canted FM state with uniform distribution of electrons. The size of the PS area is b and the size of the FM cluster in the PS area is a . Inside the FM region the parameter θ corresponds to the FM state ($\theta = 0$). In the outer region we assume $\theta = \pi$ (AFM state). We optimize the energy of the PS state with respect to the size of the PS area b and the FM cluster size a . The compression ratio ξ can be introduced here as the number of sites in the FM region divided by the total number of sites in the whole PS area.

We use an iterative self-consistent procedure to find the ground state of the system. At each step, the electronic wave functions are calculated using the direct diagonalization of the Hamiltonian (by taking into account 4 order rotation symmetry of the system). The electric potential is calculated using the electron density found at the previous iteration step. The potential has the form

$$\phi_i = \sum_j U_{ij}^C \rho_j, \quad (9)$$

where $\rho_j = \rho_j^{\text{ion}} + \rho_j^{\text{el}}$ is the charge density at site j consisting of ion and electron contributions. The ion charge density is uniform across the whole PS area and is defined by $\rho_j^{\text{ion}} = -en_0$. The electron density is given by

$$\rho_j = e \sum_k |\Psi_j^k|^2, \quad (10)$$

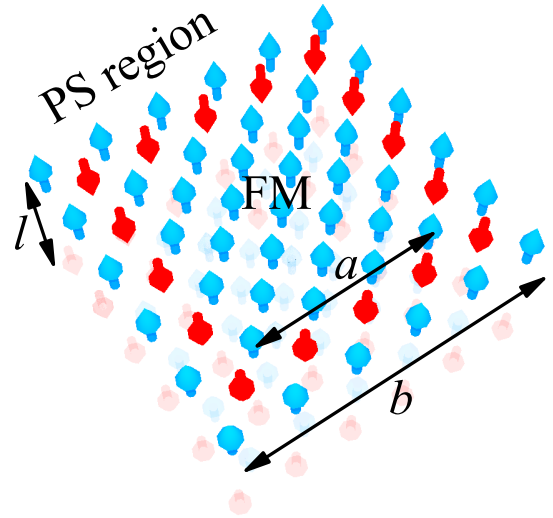


FIG. 5. Phase-separated region in a MO film. The FM region (of size a) is surrounded by the AFM area. The total size of the PS area is b . The MO film is uniform with canted AFM state outside the PS region. The thickness of the film is l . The FM cluster size varies from slice to slice due to the checkerboard ordering of magnetic moments in the AFM state.

where the summation goes over all occupied states k with the wave functions Ψ^k . The Coulomb interaction U_{ij}^C is defined as

$$U_{ij}^C = \begin{cases} \frac{1}{\tilde{\epsilon}|\mathbf{r}_i - \mathbf{r}_j|}, & i \neq j, \\ U_{ii}^C, & i = j, \end{cases} \quad (11)$$

where the effective dielectric constant is given by $\tilde{\epsilon} = (1 + \epsilon)/2$. As in the previous section we assume that the MO film is at the interface between the FE substrate and the air (or some other surrounding medium with $\epsilon = 1$). In this case the influence of the FE substrate is just the renormalization of the dielectric constant.

We assume that electron wave functions are localized at the ions. Therefore, electrons located at different sites can be considered as point charges and we have $U_{ij}^C \sim 1/|\mathbf{r}_i - \mathbf{r}_j|$. For two electrons sitting at the same site the Coulomb interaction is defined by Wannier wave functions of these electrons. The Wannier functions are not defined in the tight-binding model. Therefore, we use an additional parameter U_{ii}^C in our model to describe the on-site Coulomb repulsion. Since in our model the electrons are localized we have $U_{ii}^C < 1/(\tilde{\epsilon}\Delta)$. We show that the choice of U_{ii}^C does not change the final result qualitatively if the electron density is low. Thus, below we use $U_{ii}^C = 1/(\tilde{\epsilon}\Delta)$.

After several iterations the system reaches the equilibrium state and the energy converges to a certain value, E_{eq} . For given l , U_0 , J , n_0 , and ϵ we minimize the energy E_{eq} with respect to size of the PS region b and the size of the FM cluster a . The case $a = b$ should be considered separately since it corresponds to the uniform MO film and the energy quantization does not appear in this case. Finally, we compare the energy of the states with $a < b$ and with $a = b$ and define whether the PS occurs in the considered rectangular area.

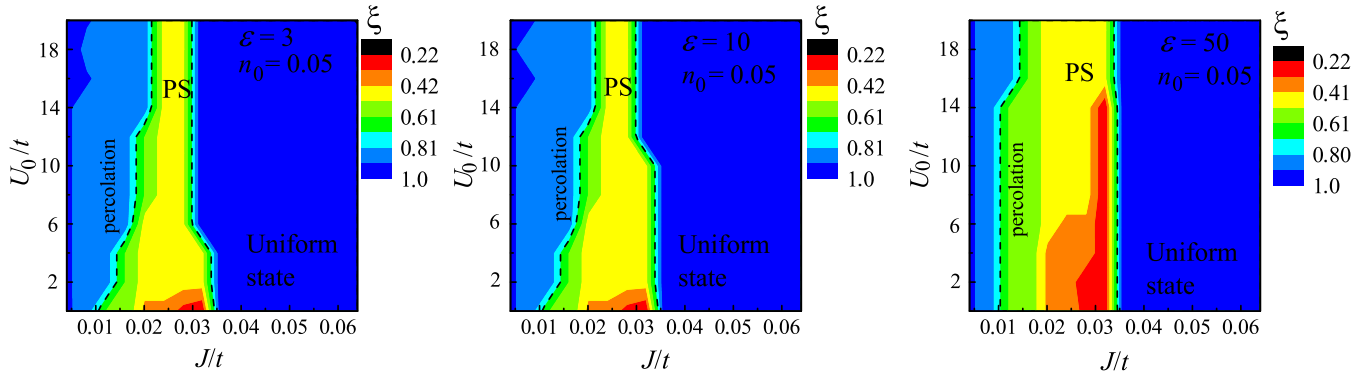


FIG. 6. Dependence of the compression ratio ξ on normalized J and U_0 for three different FE dielectric constants, $\varepsilon = 3$ (left panel), $\varepsilon = 10$ (central panel), and $\varepsilon = 50$ (right panel). The electron concentration and the MO layer thickness are fixed, $n_0 = 0.05$ and $l = 6\Delta$. The dashed line shows the compression ratio corresponding to the percolation in a two-dimensional system with random distribution of clusters.

Note again that we consider here a single PS area. However, we assume that if formation of a single PS area considered here is favorable then the whole film should transfer into the PS state with the average cluster size being a and the distance between the clusters being b . In the film with many PS regions the average cluster size and the intercluster distance are affected by the intercluster Coulomb interaction. This interaction was not taken into account here. However, this interaction is short range and does not change the result qualitatively.

For small parameter ξ the clusters are well separated in space forming the PS SPM insulating state (I + SPM). For large ξ the percolation appears and the I + SPM state transforms into the metallic FM state.

B. Phase diagram of magnetic oxides

A typical magnetic phase diagram obtained using numerical simulations is shown in Fig. 6. The equilibrium parameter ξ is shown as a function of exchange interaction J and the Coulomb energy U_0 for $n_0 = 0.05$, MO film thickness $l = 6$, and $\varepsilon = 3, 10$, and 50 . In contrast to the analytical phase diagram shown in Sec. III, here the system energy is optimized over both the characteristic FM cluster size and the AFM region size (over parameters a and b). Three cases with the same electron concentration n_0 but different dielectric constants are shown in Fig. 6.

There are two distinct areas in each phase diagram. For large J the uniform state with canted AFM order (CFM + M; blue area) is the most favorable. This is in agreement with the analytical model and the data in Fig. 2. For large J the exchange interaction becomes too strong and the energy loss due to formation of the FM cluster cannot be compensated by the energy gain due to decreasing of the electron kinetic energy [black line in Fig. 2(b)]. The uniform state does not have the insulating AFM inclusion and corresponds to the conductive state.

The second area (multicolored) corresponds to the PS state with FM cluster surrounded by the AFM insulating region. The red color shows the states with largest phase separation where $\xi \sim 0.2$. In these states the electron concentration in the FM cluster increases 5 times. However, even in this case the electron concentration is on the order of 0.25 electrons

per site such that the model is still valid. The typical size of the optimal PS region in our simulations is around 12–15 sites (involving from 500 to 900 sites per atomic layer). The compression ratio ξ decreases with increasing the Coulomb interaction since this interaction favors the uniform state. The black dashed line shows ξ at which the FM cluster relative volume corresponds to the percolation threshold. Inside this line the clusters are well separated from each other and form an independent conductive area in the insulating matrix (I + SPM). The film is an insulator in this case. Moreover, the FM clusters do not interact and the whole system is a superparamagnet. Outside the black dashed line the FM clusters overlap and form an infinite conductive FM network.

The numerical phase diagram in Fig. 6 is qualitatively similar to the phase diagram of the analytical model shown in Fig. 3. However, we did not study the metastable states numerically. Therefore, the region GUS + PS shown in Fig. 3 is absent in Fig. 6. This region is included in the uniform state area. Similarly, we do not show here the GPS + US region. It is included in the PS area.

Figure 6 has three panels showing the dependence of the phase diagram on the dielectric constant of the FE layers ε . Increasing ε increases the PS state area. Increasing the dielectric constant decreases the long-range Coulomb interaction which favors the uniform state.

Figure 7 shows the phase diagrams in the coordinates J/t vs ε for fixed $U_0/t = 10$ and electron concentration $n_0 = 0.05$ for different thicknesses $l = 2, 4$, and 6 monolayers. Increasing the FE dielectric constant ε increases the range of J where the PS state appears. This is because increasing ε enhances the screening of electric field and reduces the Coulomb interaction leading to the PS state. For TTF-CA FE the dielectric constant grows from 50 to 500 near the Curie point (see Sec. VA). Using the thin MO film ($l = 2$ monolayers) with $J = 0.035t$ one can reach the MIT and the FM \rightarrow SPM transition in the vicinity of the Curie point (black arrow on the right panel in Fig. 7).

The dependence on the thickness of the MO layer is not very pronounced in the studied region. We investigate the MO films with different thicknesses up to 10 monolayers and do not find any big difference (compare three panels in Fig. 7). The only consequence of the thickness increase is

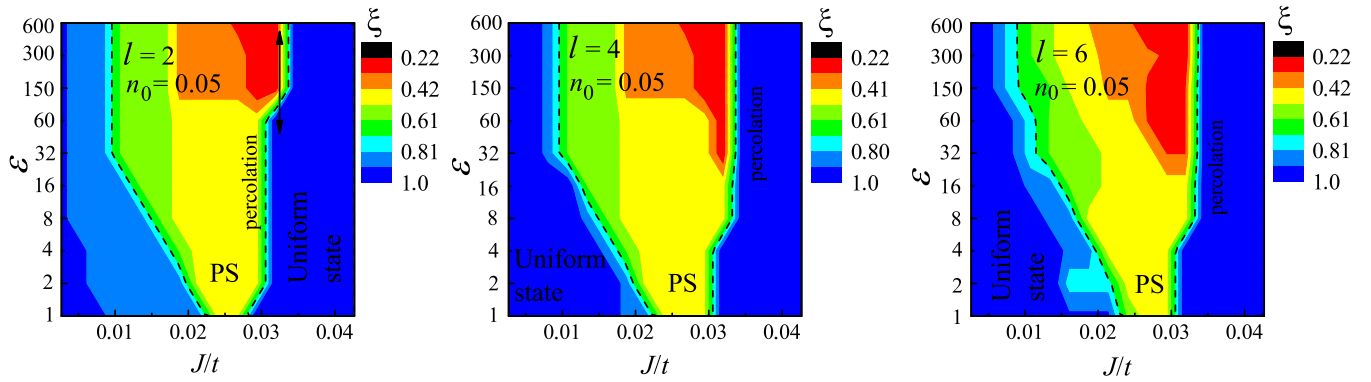


FIG. 7. Dependence of the compression ratio ξ on the normalized exchange coupling J and the FE dielectric constant ε for three different MO layer thicknesses, $l = 2$ (left panel), $l = 4$ (central panel), and $l = 6$ (right panel). The electron concentration and the Coulomb interaction parameters are fixed, $n_0 = 0.05$ and $U_0/t = 10$. The dashed line shows the compression ratio corresponding to the percolation in a two-dimensional system with random distribution of clusters. The black arrow in the left panel shows the system trajectory corresponding to the dielectric constant variation near the Curie point in TTF-CA.

the decrease of the induced charge due to FE polarization switching, $\Delta n_0 \sim 1/l$.

Figure 8 shows the phase diagram of the MO film for larger Coulomb interaction, $U_0 = 20t$, and larger electron concentration, $n_0 = 0.075$. The position of PS states in this case moves to higher values of the dielectric constants. The transition between homogeneous and PS states appears at higher ε . In artificial FEs such as $\text{PbTiO}_3/\text{CaTiO}_3$ the dielectric constant is not very large and decreases from 400 to 100 under the influence of an electric field. Using the MO with $J \approx 0.045t$ one can obtain the MIT and FM \rightarrow SPM transitions applying the electric field. The arrow in Fig. 8 shows the system trajectory in the parameter space when the electric field is applied to the $\text{PbTiO}_3/\text{CaTiO}_3$ substrate.

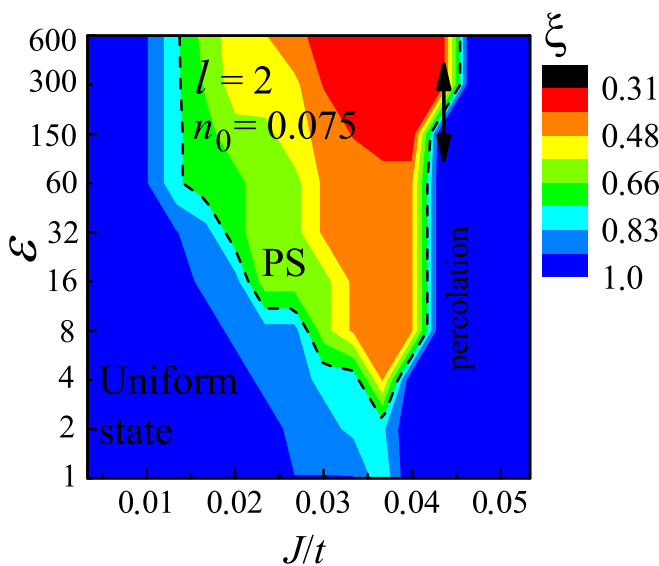


FIG. 8. Dependence of the compression ratio ξ on the normalized exchange coupling J and the FE dielectric constant ε for $l = 2$, $n_0 = 0.075$, and $U_0/t = 20$. The dashed line shows the compression ratio corresponding to the percolation in a two-dimensional system with random distribution of clusters. The black arrow shows the system trajectory corresponding to the reduction of dielectric constant due to applied electric field to $\text{PbTiO}_3/\text{CaTiO}_3$ FE.

Switching the FE polarization P_0 also influences the state of MO film. Indeed, switching polarization from $-P_0$ to P_0 will change the surface charge density by $2P_0$ leading to variation of the electron concentration by $\Delta n_0 = 2P_0\Delta^2/l$ (for polarization direction being perpendicular to the MO film plane).

Figure 9 shows the change of the MO film state with electron concentration. For low electron concentration the homogeneous state is more favorable. Therefore, to create the PS state the electron concentration should be large enough. Increasing the electron concentration increases the parameter region with PS state. At that the compression ratio increases with n_0 since the Coulomb interaction increases. Switching of the FE polarization can change n_0 by 0.05 electron per site for thin film. The arrow in Fig. 9 shows the system trajectory in the parameter space for such a variation of n_0 .

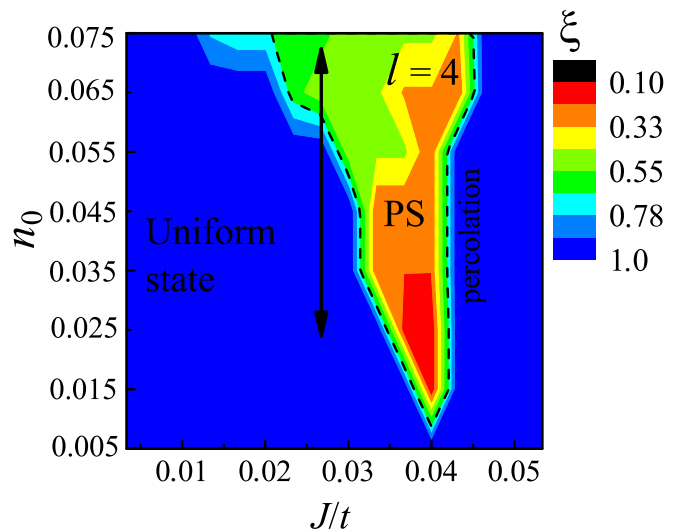


FIG. 9. Dependence of the compression ratio ξ on the normalized exchange coupling J and the electron concentration n_0 for $l = 4$, $\varepsilon = 30$, and $U_0/t = 10$. The dashed line shows the compression ratio corresponding to the percolation in a two-dimensional system with random distribution of clusters. The black arrow shows the system trajectory corresponding to the FE polarization switching.

V. DISCUSSION

A. Suitable materials

As we discussed in the previous sections, variation of the FE substrate properties may induce the MIT and SFM \rightarrow SPM transitions. Here we discuss some relevant FE materials. One way to tune the FE dielectric constant is varying temperature. For example, in TTF-CA FE the dielectric constant ϵ rises from 50 to 500 in the vicinity of the Curie temperature which is on the order of 100 K [33]. In PMN-PT the dielectric constant grows from 2000 to 20000 [34] in the vicinity of the phase transition. However, the Curie temperature of this material is quite high ($T_C \approx 200^\circ\text{C}$). The magnetic phase transition temperature in MO depends on the doping level. At low doping (current work) the magnetic transition occurs mostly at low temperatures. For LaCaMnO_3 the magnetic state occurs below 150 K [35], for NdSrMnO_3 below 100 K [21].

Another way to control the system is to apply an electric field pulse switching the FE polarization. The typical magnitude of polarization in FEs is on the order of $10 \mu\text{C}/\text{cm}^2$. Taking into account the typical lattice constant of MO on the order of 0.5 nm one can estimate the surface charge density induced by the FE at the level of 0.3 electrons per the surface area of a unit cell. For film with the thickness of 6 monolayers the charge density per one site is $\Delta n_0 = 0.025$. In PMN-PT FE the polarization is $P_0 \approx 20 \mu\text{C}/\text{cm}^2$ [34] leading to $\Delta n_0 = 0.05$. Some FE materials have higher polarization but some have much a smaller one. For example, Li-doped ZnO has a polarization on the order of $0.2 \mu\text{C}/\text{cm}^2$ [36]. P(VDF-TrFE) also demonstrates low polarization at the level of $0.1 \mu\text{C}/\text{cm}^2$ [37]. $\text{Sr}_2\text{Nb}_2\text{O}_7$ FE has a saturation polarization on the order of $2 \mu\text{C}/\text{cm}^2$.

The third way to change the parameters of the FE substrate is to apply a constant electric field changing the dielectric constant. In SrBiTiO_3 and KTiO_3 the dielectric constant decreases from 3000 to 1000 in a field of 60 kV/cm at low temperatures (around 50 K) [38]. Such a field produces a surface charge on the order of $5 \mu\text{C}/\text{cm}^2$ ($\Delta n_0 \approx 0.01$ for a 6-monolayer film). In HfZrO_2 the saturation polarization can be on the order of $15 \mu\text{C}/\text{cm}^2$ ($\Delta n_0 \approx 0.035$). At that the variation of the dielectric constant is between 30 and 40 at room temperature [39]. In artificial superlattices $\text{PbTiO}_3/\text{CaTiO}_3$ the dielectric constant varies from 400 to 100 with electric field [40]. The variation happens in a field on the order of 1 MV/cm (producing a charge density on the order of $n_0 = 0.02$ for a 6-monolayer MO film).

B. Percolation problem

In two-dimensional systems with random distribution of clusters the percolation occurs when the relative area of the clusters reaches the critical value, $\xi_{\text{cr}} = 0.68\%$ [41]. Note that the compression ratio in our consideration is exactly the relative area occupied by the FM clusters. If we consider the FM droplets as independent then the percolation will appear around the critical value of ξ .

Note, however, that negatively charged FM droplets should repel each other. Thus, generally they cannot be considered

as independent objects. This should lead to formation of a regular lattice of FM regions. Since in such a state there are insulating areas between droplets the state of the whole system can be considered as insulating and superparamagnetic. Thus, the interaction between FM droplets can increase the critical value of ξ at which percolation appears.

On the other hand, there could be some pinning sites or defects that fix position of the FM droplets. If the pinning potential is larger than the Coulomb repulsion between the droplets the random distribution of droplets is more realistic. The influence of cluster interaction and pinning of clusters on the overall system state should be studied separately and is beyond the scope of the present work.

C. Other ME effects in the system

Finite electric voltage applied to the FE induces strain in the FE leading to the appearance of finite strain in the MO film. The strain also modifies magnetic and transport properties of the MO films [15,42]. We do not take this effect into account in our model. We assume that one can choose a FE with weak piezoelectric effect but large variations of the dielectric constant and high electric polarization. For example LiNbO_3 produces small deformation (10 times smaller than PMN-PT or BTO) but has the same polarization as PMN-PT.

We consider the case of electric polarization being perpendicular to the MO film plane. In this case the charge accumulation effect is non-negligible. At that in uniaxial FEs (such as LiNbO_3) one can make a cut along the polarization axis (nonpolar cut). In this case the FE polarization does not influence the MO film. In contrast, the effect of the Coulomb interaction screening is still present. Thus, to observe the effect related to the FE dielectric constant alone one needs to use a nonpolar cut of the FE. One can measure the temperature dependence of the conductivity or magnetization in the vicinity of the FE Curie point.

VI. CONCLUSION

We theoretically studied the hybrid system consisting of a MO thin film on top of a FE substrate. We showed that the FE dielectric constant and polarization essentially influence the MO film properties. In particular, changing either the FE dielectric constant or polarization one can switch the MO film state from conductive to insulating and vice versa. Simultaneously, the FM to SPM transition occurs. The FE dielectric constant and polarization can be tuned by either temperature or electric field. We used both the analytical model and numerical simulations to tackle the problem and discussed suitable FE materials.

ACKNOWLEDGMENTS

This research was supported by NSF under Cooperative Agreement Award No. EEC-1160504. O.U. was supported by the Foundation for the Advancement of Theoretical Physics and Mathematics BASIS (Grant No. 18-1-3-32-1) and Russian Foundation for Basic Researches (Grant No. 18-32-20036).

- [1] Z. Li, Y. Zhang, Y. Huang, C. Wang, X. Zhang, Y. Liu, Y. Zhou, W. Kang, S. C. Koli, and N. Lei, *J. Magn. Magn. Mater.* **455**, 19 (2018).
- [2] F. Zavaliche, T. Zhao, H. Zheng, F. Straub, M. P. Cruz, P.-L. Yang, D. Hao, and R. Ramesh, *Nano Lett.* **7**, 1586 (2007).
- [3] J. J. Yang, Y. G. Zhao, H. F. Tian, L. B. Luo, H. Y. Zhang, Y. J. He, and H. S. Luo, *Appl. Phys. Lett.* **94**, 212504 (2009).
- [4] H. Zheng, J. Wang, S. E. Lofland, Z. Ma, L. Mohaddes-Ardabili, T. Zhao, L. Salamanca-Riba, S. R. Shinde, S. B. Ogale, F. Bai, D. Viehland, Y. Jia, D. G. Schlom, M. Wuttig, A. Roytburd, and R. Ramesh, *Science* **303**, 661 (2004).
- [5] S. Sahoo, S. Polisetty, C.-G. Duan, S. S. Jaswal, E. Y. Tsymbal, and C. Binek, *Phys. Rev. B* **76**, 092108 (2007).
- [6] J.-M. Hu, T. Yang, J. Wang, H. Huang, J. Zhang, L.-Q. Chen, and C.-W. Nan, *Nano Lett.* **15**, 616 (2015).
- [7] T. Brintlinger, S.-H. Lim, K. H. Baloch, P. Alexander, Y. Qi, J. Barry, J. Melngailis, L. Salamanca-Riba, I. Takeuchi, and J. Cumings, *Nano Lett.* **10**, 1219 (2010).
- [8] M. Liu, Z. Zhou, T. Nan, B. M. Howe, G. J. Brown, and N. X. Sun, *Adv. Mater.* **25**, 1435 (2013).
- [9] S. Zhang, Y. G. Zhao, P. S. Li, J. J. Yang, S. Rizwan, J. X. Zhang, J. Seidel, T. L. Qu, Y. J. Yang, Z. L. Luo, Q. He, T. Zou, Q. P. Chen, J. W. Wang, L. F. Yang, Y. Sun, Y. Z. Wu, X. Xiao, X. F. Jin, J. Huang, C. Gao, X. F. Han, and R. Ramesh, *Phys. Rev. Lett.* **108**, 137203 (2012).
- [10] Y. Yamasaki, S. Miyasaka, Y. Kaneko, J.-P. He, T. Arima, and Y. Tokura, *Phys. Rev. Lett.* **96**, 207204 (2006).
- [11] L. O. Mair, L. J. Martinez-Miranda, L. K. Kurihara, A. Nacev, R. Hilaman, S. Chowdhury, S. Jafari, S. Ijanaten, C. da Silva, J. Baker-McKee, P. Y. Stepanov, and I. N. Weinberg, *AIP Adv.* **8**, 056731 (2018).
- [12] C. Thiele, K. Dorr, O. Bilani, J. Rodel, and L. Schultz, *Phys. Rev. B* **75**, 054408 (2007).
- [13] P. M. Leufke, R. Kruk, R. A. Brand, and H. Hahn, *Phys. Rev. B* **87**, 094416 (2013).
- [14] H. Lu, T. A. George, Y. Wang, I. Ketsman, J. D. Burton, C.-W. Bark, S. Ryu, D. J. Kim, J. Wang, C. Binek, P. A. Dowben, A. Sokolov, C.-B. Eom, E. Y. Tsymbal, and A. Gruverman, *Appl. Phys. Lett.* **100**, 232904 (2012).
- [15] Z. G. Sheng, J. Gao, and Y. P. Sun, *Phys. Rev. B* **79**, 174437 (2009).
- [16] C. A. F. Vaz, J. Hoffman, Y. Segal, J. W. Reiner, R. D. Grober, Z. Zhang, C. H. Ahn, and F. J. Walker, *Phys. Rev. Lett.* **104**, 127202 (2010).
- [17] C. A. F. Vaz, *J. Phys.: Condens. Matter* **24**, 333201 (2012).
- [18] O. G. Udalov, N. M. Chtchelkatchev, and I. S. Beloborodov, *J. Phys.: Condens. Matter* **27**, 186001 (2015).
- [19] O. G. Udalov and I. S. Beloborodov, *J. Phys.: Condens. Matter* **29**, 155801 (2017).
- [20] O. G. Udalov, N. M. Chtchelkatchev, and I. S. Beloborodov, *Phys. Rev. B* **89**, 174203 (2014).
- [21] M. B. Salamon and M. Jaime, *Rev. Mod. Phys.* **73**, 583 (2001).
- [22] E. Dagotto, T. Hotta, and A. Moreo, *Phys. Rep.* **344**, 1 (2001).
- [23] A. P. Ramirez, *J. Phys.: Condens. Matter* **9**, 8171 (1997).
- [24] M. Uehara, S. Mori, C. H. Chen, and S. W. Cheong, *Nature (London)* **399**, 560 (1999).
- [25] A. J. Millis, B. I. Shraiman, and R. Mueller, *Phys. Rev. Lett.* **77**, 175 (1996).
- [26] A.-M. Haghiri-Gosnet and J.-P. Renard, *J. Phys. D: Appl. Phys.* **36**, R127 (2003).
- [27] E. Dagotto, J. Burgy, and A. Moreo, *Solid State Commun.* **126**, 9 (2003).
- [28] M. Kagan, D. Khomskii, and M. Mostovoy, *Eur. Phys. J. B* **12**, 217 (1999).
- [29] A. O. Sboychakov, K. I. Kugel, A. L. Rakhmanov, and D. I. Khomskii, *Phys. Rev. B* **80**, 024423 (2009).
- [30] M. Y. Kagan, A. V. Klaptsov, I. V. Brodsky, K. I. Kugel, A. O. Sboychakov, and A. L. Rakhmanov, *J. Phys. A: Math. Gen.* **36**, 9155 (2003).
- [31] M. Y. Kagan and K. I. Kugel', *Phys. Usp.* **44**, 553 (2001).
- [32] O. G. Udalov and I. S. Beloborodov, *Phys. Rev. B* **96**, 024204 (2017).
- [33] K. Kobayashi, S. Horiuchi, R. Kumai, F. Kagawa, Y. Murakami, and Y. Tokura, *Phys. Rev. Lett.* **108**, 237601 (2012).
- [34] P. Kumar, S. Sharma, O. Thakur, C. Prakash, and T. Goel, *Ceram. Int.* **30**, 585 (2004).
- [35] P. Schiffer, A. P. Ramirez, W. Bao, and S.-W. Cheong, *Phys. Rev. Lett.* **75**, 3336 (1995).
- [36] X. Wang, Z. Wu, J. Webb, and Z. Liu, *Appl. Phys. A* **77**, 561 (2003).
- [37] V. Bharti and Q. M. Zhang, *Phys. Rev. B* **63**, 184103 (2001).
- [38] C. Ang and Z. Yu, *Phys. Rev. B* **69**, 174109 (2004).
- [39] J. Muller, T. S. Boscke, U. Schroder, S. Mueller, D. Brauhaus, U. Bottger, L. Frey, and T. Mikolajick, *Nano Lett.* **12**, 4318 (2012).
- [40] J. Sinsheimer, S. J. Callori, B. Bein, Y. Benkara, J. Daley, J. Coraor, D. Su, P. W. Stephens, and M. Dawber, *Phys. Rev. Lett.* **109**, 167601 (2012).
- [41] J. Quintanilla, S. Torquato, and R. M. Ziff, *J. Phys. A: Math. Gen.* **33**, L399 (2000).
- [42] R. K. Zheng, Y. Wang, H. L. W. Chan, C. L. Choy, and H. S. Luo, *Phys. Rev. B* **75**, 212102 (2007).